Contrib Mineral Petrol (2006) 151: 600–614
DOI 10.1007/s00410-006-0073-8

ORIGINAL PAPER

Kurt J. Steffen · Jane Selverstone

Retrieval of *P–T* information from shear zones: thermobarometric consequences of changes in plagioclase deformation mechanisms

Received: 28 April 2005 / Accepted: 31 January 2006 / Published online: 21 March 2006

Abstract Changes in deformation mechanism coupled with spatial and temporal variations in reaction rates can result in preservation of disequilibrium mineral compositions in rocks affected by synmetamorphic shearing. Thermobarometric calculations on such rocks may thus yield meaningless results. We use Garbenschiefer samples from a shear zone in the Eastern Alps to study the effects of different deformational processes on calculated pressures and temperatures in samples that experienced the same overall PTt history. We focus on plagioclase, which accommodates strain by a variety of deformation mechanisms and is a key mineral in many thermobarometers. Plagioclase that deformed largely via dislocation creep mechanisms shows concentric chemical zoning, whereas plagioclase that experienced dissolution-precipitation creep preserves complex zoning. Rim compositions in the latter domains are not necessarily the youngest compositions, nor did they typically equilibrate with other phases in the assemblage. The timing of hornblende breakdown reactions relative to changes in plagioclase deformation mechanism also affected chemical zoning. Samples that escaped shear strain while near the thermal maximum yield internally consistent thermobarometric results, whereas samples that experienced shearing near the thermal maximum yield scattered results. Some of the variability in the results likely represents real differences in the *P–T* conditions at which equilibration occurred during deformation. However, much of the variability represents spurious results obtained by pairing mineral compositions that were never in equilibrium with one another. Extraction of useful *P–T* information from samples that experienced synmetamorphic deformation requires careful documentation of the relationships between deformation mechanisms and chemical zoning in order to select appropriate mineral compositions for thermobarometric calculations.

Electronic Supplementary Material Supplementary material is available for this article at http://dx.doi.org/10.1007/s00410-006-0073-8 and is accessible for authorized users.

Communicated by T. L. Grove

K. J. Steffen · J. Selverstone
Department of Earth and Planetary Sciences,
University of New Mexico, Albuquerque, NM 87131, USA

K. J. Steffen (✉)
ExxonMobil Upstream Research Company,
P.O. Box 2189, Houston, TX 77252, USA
E-mail: kurt.j.steffen@exxonmobil.com
Tel.: +1-713-4316541
Fax: +1-713-4317279

Introduction

In rocks containing zoned minerals, the selection of appropriate compositions to use in thermobarometric calculations typically contributes the greatest uncertainty to calculated *P–T* conditions (Kohn and Spear 1991). The mechanisms responsible for chemical zoning must be understood in order to properly select compositions for *P–T* calculations. The chemical analyses used in the calculations must represent compositions that existed in equilibrium with one another (“local equilibrium assumption”), and if possible, the processes that led to equilibration should also be identified. In some samples, preserved mineral compositions never equilibrated with one another, and these samples will always lead to spurious thermobarometric results.

Development of chemical zoning in minerals solely due to metamorphic processes can result from changes in external conditions (e.g., Tracy 1976; Spear and Selverstone 1983; Frost and Tracy 1991) or changes in the effective bulk composition of the chemical system (Stüwe 1997) during mineral growth. Changes in the effective bulk composition during mineral growth may relate to metasomatism (Wintsch and Knipe 1983; Yardley et al. 1991) or to the partitioning of components into the relatively non-reactive cores of mineral phases, thus changing

the composition of the system available for chemical reaction (Tracy 1982; Chernoff and Carlson 1997).

Many studies show that deformation can also affect the rates and mechanisms of chemical equilibration (Brodie 1981; Brodie and Rutter 1985; Koons et al. 1987; Tullis and Yund 1991; Yund and Tullis 1991; Tullis et al. 1996; Farver and Yund 1999; Stünitz and Tullis 2001; Baxter and DePaolo 2004). For example, changes in plagioclase composition aided by grain-boundary migration recrystallization have been documented experimentally by Tullis and Yund (1991) and in natural samples by Stünitz (1998). Because most metamorphic rocks exist in a state of partial chemical disequilibrium (Carlson 2002), enhanced chemical kinetics related to deformational processes could exert a strong control on chemical communication between minerals and, by extension, on pressures and temperatures calculated from thermobarometry.

Processes that increase rates of chemical equilibration during deformation include (Yund and Tullis 1991; Tullis et al. 1996): (1) grain-size reduction, which increases mineral surface area and decreases mean distances for volume diffusion; (2) motion of high-angle grain boundaries during recrystallization-accommodated dislocation creep; and (3) changes in grain-boundary fluid distribution, which can enhance strain accommodation via dissolution and reprecipitation. After deformation ceases, due either to changes in the far-field stress field or to rheological changes that partition strain into other domains, deformation-enhanced rates of chemical equilibration will slow. Local variations in the timing of deformation may result in significant differences in the P–T conditions at which equilibration occurs. Thermobarometric calculations may thus yield accurate but widely varying pressures and temperatures for samples that followed the same PTt path. Strain heterogeneities and changes in deformation mechanism can also lead to variations in reaction kinetics that allow non-equilibrium mineral compositions to be preserved. Pressures and temperatures calculated from these rocks may be spurious.

The Greiner shear zone in the Tauern Window, Eastern Alps, provides an excellent natural laboratory for studying the effects of coupled deformation and metamorphism on calculated P–T conditions. The regional PTt history is well constrained by previous work and provides a reference frame for interpretation of the data. Large local variations in strain-accommodation mechanisms and preserved textures allow calculated P–T conditions to be evaluated in samples that experienced different deformational processes, but similar overall PTt history. This study documents the roles that structural history and plagioclase deformation mechanisms play in controlling mineral equilibration within the shear zone. Knowledge of these controls is essential to the selection of appropriate mineral compositions for use in thermobarometric calculations and for interpreting the results of those calculations.

Regional geology and previous work

The Greiner shear zone is a subvertical, ENE-striking zone of concentrated pure and simple shear located in the western Tauern Window along the Austrian-Italian border (Fig. 1). The dominant metamorphism and deformation in the area relate to the Cretaceous-Tertiary closure of the Neo-Tethys ocean basin and collision of the Eurasian plate with the Adriatic plate. This collision resulted in west- to north-directed emplacement of Adriatic nappes over oceanic and thinned continental margin rocks now exposed in the Tauern Window. Subsequent transpressional motion of the Adriatic plate led to east–west extension of overthickened crust and exhumation of the Tauern Window (Selverstone 1988; Ratschbacher et al. 1991; Lammerer and Weger 1998).

There are three major lithotectonic packages present in the Tauern Window (Morteani 1974; Selverstone et al. 1984). The structurally lowest, the Hercynian-age Zentralgneis (ZG), consists of granodiorite and tonalite that display textures ranging from igneous to gneissic. Structurally above the Zentralgneis is the Lower Schieferhülle (LSH), which consists of a lower, autochthonous, Paleozoic sequence (PLSH) and an upper, parautochthonous sequence that includes rocks of Mesozoic and Tertiary age (MLSH). The PLSH predates emplacement of the Zentralgneis and is dominantly composed of interleaved aluminous amphibolite (Garbenschiefer), biotite schist, and graphitic schist. The MLSH consists of metaconglomerate, quartzite, marble, and pelitic and calcareous schists that have correlatives throughout the Alps. The structurally highest package, the Upper Schieferhülle (USH), is an allochthonous sequence of greenstone, marble, calcareous and pelitic schists derived from the Neo-Tethys basin.

The Greiner shear zone is located in synformal position between two basement (ZG)-cored antiforms and is defined by an ENE-striking subvertical foliation formed by extreme transposition of earlier fabrics. The Greiner shear zone cuts all structural levels, indicating that it was active after Alpine nappe emplacement, although some earlier motion cannot be ruled out. Metamorphic grade within the synform increases from west (upper greenschist) to east (amphibolite facies).

This study primarily focuses on coarse-grained, hornblende Garbenschiefer horizons within the PLSH. The hornblende Garbenschiefer is composed of large (up to 20 cm in length), radiating hornblende porphyroblasts that typically cross both the lineation and the foliation, although in some horizons hornblende lies within foliation planes and has grown or been rotated to define a lineation. Typical mineral assemblages include hornblende + plagioclase + quartz + epidote + ilmenite ± garnet ± biotite ± white mica ± chlorite ± staurolite ± kyanite ± rutile (see Selverstone et al. 1984, for details). Garbenschiefer is most abundant in the PLSH, but also occurs in some areas of the MLSH and highly

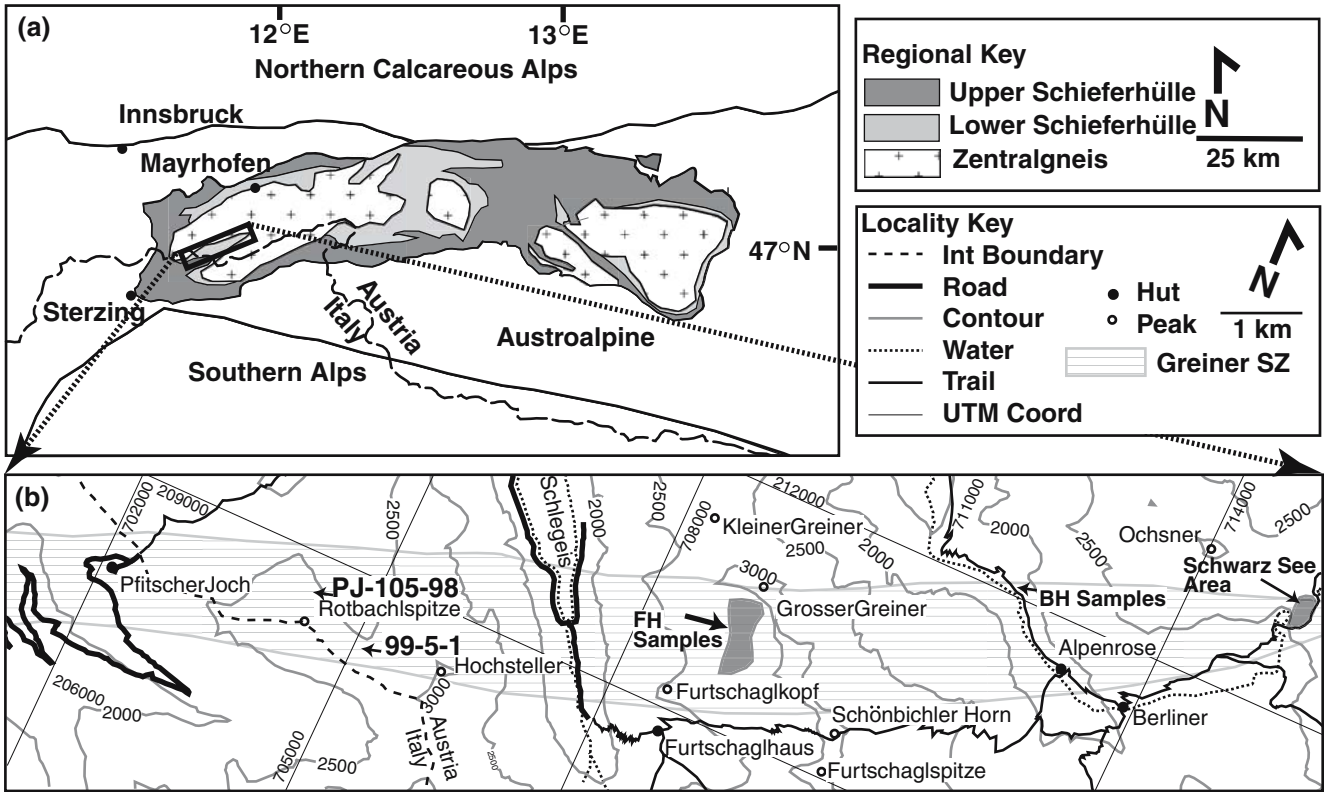

Fig. 1 **a** Map showing location of the Tauern tectonic window in the eastern Alps. **b** Detail of study area showing extent of Greiner shear zone and sample localities

strained domains in the ZG. In the PLSH, Garbenschiefer is interlayered with foliated biotite schist at the scale of centimeter to meter. Small amounts of fine-grained amphibolite that lack radiating bundles of hornblende also are present in the PLSH; these typically also lack the aluminous minerals (garnet, staurolite, kyanite) that characterize many Garbenschiefer horizons. Fine-grained amphibolite is most abundant along the northern margin of the PLSH portion of the Greiner shear zone where a large strain gradient exists between the PLSH and the relatively undeformed ZG north of the shear zone.

Hornblende-consuming reactions occurred locally within some portions of the Greiner synform and shear zone, as evidenced by the presence of biotite-rich pseudomorphs after hornblende. The pseudomorphs record reaction between hornblende and white mica to produce biotite + plagioclase + H_2O ± garnet ± staurolite ± chlorite in rocks with relatively low a_{H_2O} (Selverstone and Munoz 1987). In some areas, strain localization during or after pseudomorph development resulted in pervasive transformation of Garbenschiefer into biotite schist (Selverstone 1993; Steffen et al. 2001).

Quantitative *P–T* paths from PLSH samples in the western and central parts of the study area show nearly isothermal decompression from 10 to ~4 kbar at ~550°C (Selverstone et al. 1984; Selverstone 1985). These paths were based in part on data from zoned minerals in kyanite- and staurolite-bearing hornblende Garbenschiefer from the Greiner zone. Maximum temperatures increase by about 50°C towards the easternmost sample localities shown in Fig. 1.

The Selverstone et al. (1984) study focused on Garbenschiefer with no obvious pseudomorphs after hornblende. The samples in that study were selected in part for their lack of obvious shear fabrics, although subsequent work (Steffen et al. 2001) has shown that development of the Garbenschiefer texture is favored by synmetamorphic shearing. Rim thermobarometry and Gibbs method results obtained by Selverstone et al. (1984) showed a high degree of consistency among samples. Owing to the presence of aluminous minerals such as staurolite and kyanite, the samples used by Selverstone et al. (1984) had unusually low thermodynamic variance for amphibolites. Arnold et al. (2000) demonstrated that coexistence of these aluminous phases with hornblende relates both to compositional factors and to the region of *P–T* space traversed by the rocks. In general, the kyanite stability field for "aluminous" amphibolites expands to a wider range of bulk compositions at higher pressures. However, it is important to note that the model of Arnold et al. (2000) does not include potassium, which precludes the consideration of the biotite and white mica equilibria that are of critical importance in the Greiner shear zone.

For this study, we sampled a much broader array of textural types than those considered by Selverstone et al. (1984), including stable hornblende Garbenschiefer, samples with varying degrees of pseudomorph formation, and biotite schists in which most traces of the prior Garbenschiefer assemblage and texture were destroyed. Our intention was to obtain a wide range of deformational features and mineral assemblages in order to evaluate the influence of different deformational and metamorphic processes on calculated *P–T* conditions. Most samples have a higher thermodynamic variance than the Selverstone et al. (1984) suite, and the samples also exhibit a wider variety of deformation mechanisms and chemical zoning features.

Deformation history and rheological heterogeneity in the Greiner shear zone

Different textures and lithologies are preserved in discontinuous lenses that are centimeters thick and extend along strike for centimeters to tens of meters within the PLSH portions of the shear zone (Fig. 2a). The penetrative foliation generally conceals evidence of early folding in the PLSH, but rare folded quartz veins (Fig. 2b) are locally apparent (e.g., FH sample area, Fig. 1b). These quartz veins are characterized by upright, open to tight folds with axes that plunge shallowly to the west, subparallel to the dominant Greiner shear zone lineation; the axial plane of the folds is coincident with the shear foliation. Folded PLSH, including Garbenschiefer (Fig. 2c), is locally exposed in low-strain areas of the Greiner shear zone in the FH sample area and also to the ESE of Pfitscher Joch (Fig. 1b). Fold orientations in these localities are similar to those observed in the quartz veins; these folds are correlative with regional F_3 folding identified by Lammerer (1988).

Two different groups of folds occur in the easternmost PLSH exposures in the Greiner synform (Schwarz See area, Fig. 1b). The dominant group is upright, with axial planes that strike ENE and fold axes that plunge shallowly to the west (Fig. 2d). The similarity in orientation and style of these folds to those described above indicates that these are F_3 folds. Tight, recumbent F_2 folds with N- or S-plunging axes are only locally present and are refolded by the F_3 folds.

Initial development of the Garbenschiefer assemblage and texture occurred in some domains during D_2 and in other domains during formation of the later, highly transposed D_3 deformation (Fig. 2a, c). Once the Garbenschiefer texture developed in a given horizon, subsequent strain was partitioned into weaker areas, such as biotite-rich domains and regions of pseudomorph

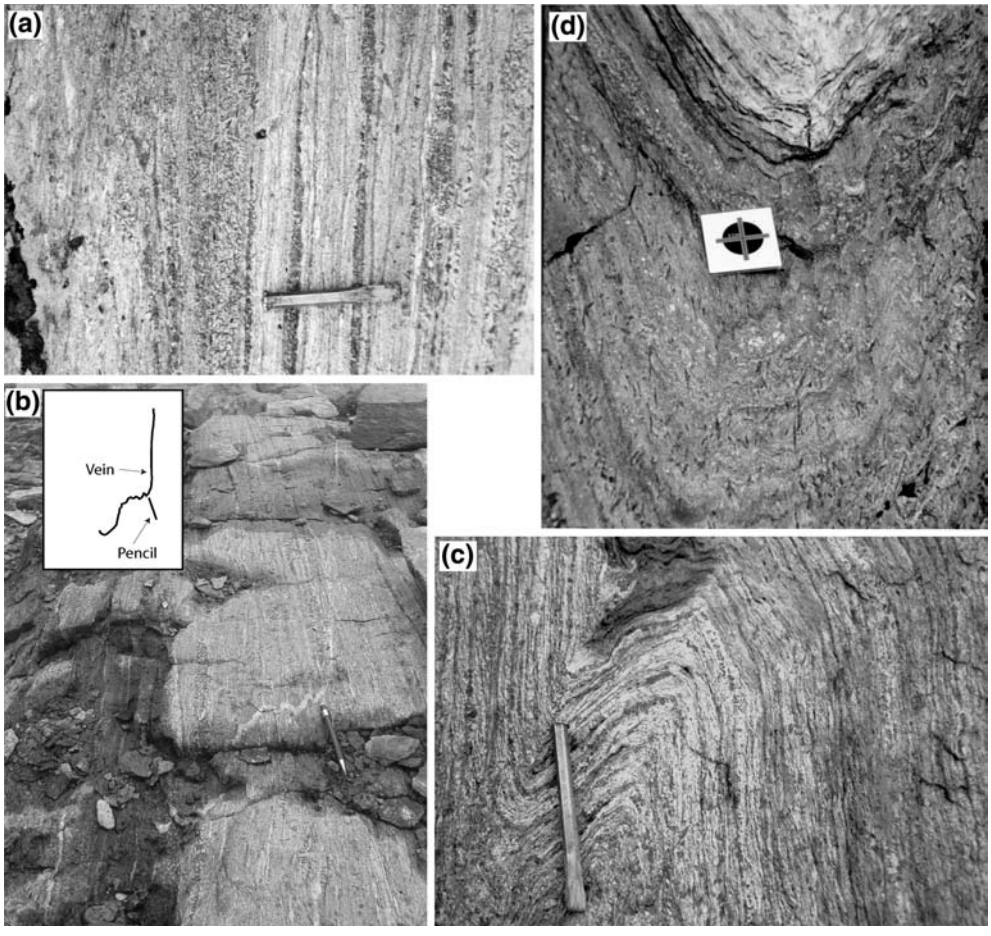

Fig. 2 Field photos of diachronous Garbenschiefer development. **a** Elongate bands of hornblende Garbenschiefer interspersed with biotite schist horizons in S_3. This is the dominant texture within Greiner shear zone. **b** Quartz veins showing upright F_3 folds, in contrast to transposed foliation in surrounding Garbenschiefer and biotite schist. **c** Garbenschiefer preserved in foliation that was folded by F_3. **d** Garbenschiefer overprinting hinge of upright D_3 folds. *Black circle* is 10 cm in diameter

formation (Steffen et al. 2001). Episodes of chemical reaction and equilibration during deformation thus do not necessarily represent event markers throughout the entire shear zone: rocks with similar textures that are in close proximity to one another could have equilibrated under different external conditions. This potential for diachronous equilibration as a function of strain localization greatly complicates the interpretation of thermobarometric results from shear zones that were active under changing P–T conditions.

Plagioclase deformation mechanisms and development of chemical zoning

Plagioclase types

In the Greiner PLSH samples, plagioclase plays a key role in recording interactions between deformational and metamorphic processes, and we focus on it for the following reasons: (1) Plagioclase is abundant in all of

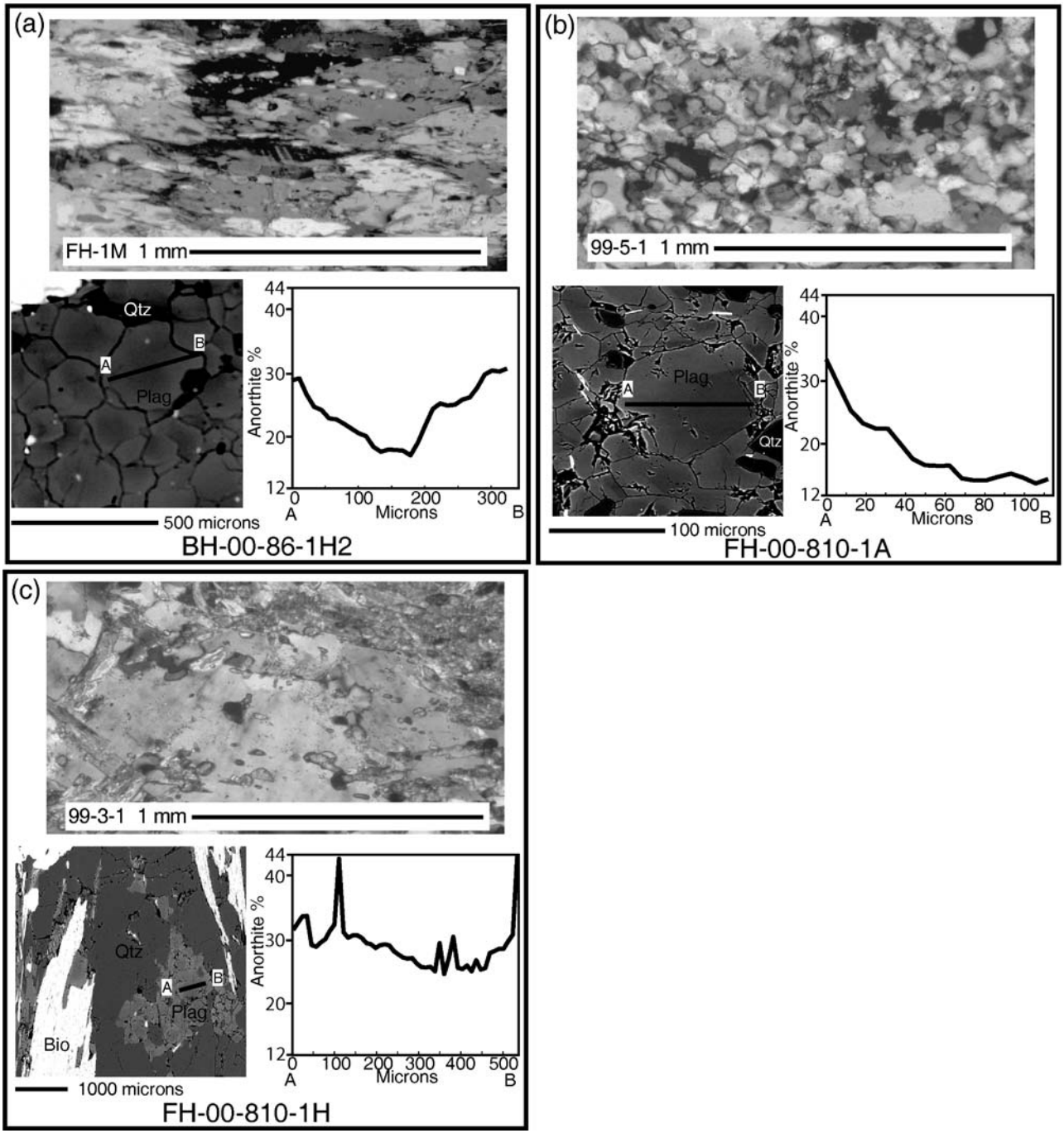

Fig. 3 Photomicrographs, BSE images and quantitative microprobe traverses for plagioclase. **a** Type A plagioclase. **b** Type B plagioclase. **c** Type C plagioclase

the relevant rock types (Garbenschiefer, pseudomorph-rich rocks, and interlayered biotite schists). (2) Plagioclase constitutes an important phase in many thermobarometers. (3) Plagioclase compositions and zoning patterns provide data on the metamorphic conditions under which plagioclase grew and/or equilibrated. (4) Much is known about the mechanisms by which plagioclase deforms under both experimental and natural conditions, thus allowing us to tie the metamorphic history to the rheologic evolution of the Greiner zone.

Based on textural and compositional characteristics, plagioclase from the Greiner zone was separated into three different types:

Type A plagioclase is coarse-grained (≥100 μm) and shows radially concentric zoning from core compositions of $An_{5–20}$ towards rim compositions of $An_{25–33}$ (Fig. 3a). Optically visible subgrains are evident in some grains. In most samples, Type A plagioclase exhibits a prominent shape-preferred orientation and a moderately well-developed lattice-preferred orientation (as observed with a gypsum plate). Type A is the dominant plagioclase type in some hornblende Garbenschiefer samples and is also locally present in pseudomorph-bearing samples and in biotite schist domains.

Type B plagioclase is typified by complexly zoned grains (Fig. 3b). Grain size varies widely (20–200 μm), but is generally less than 50 μm. Compositions range from An_{10} to An_{40}, but zoning is non-concentric with sharp truncations across which compositions can change by 10–15 mol% over distances of 5–10 μm within individual grains. Compositional heterogeneity is also invariably present between neighboring grains. This plagioclase type shows little to no shape-preferred orientation and no lattice-preferred orientation, and has very low dislocation densities (Steffen et al. 2001). Type B plagioclase is common in Garbenschiefer horizons and locally in biotite schists within the Greiner shear zone.

Type C plagioclase shows a wide range in grain sizes (20–300 μm) and is generally more An rich ($An_{25–40}$) than the other types (Fig. 3c). Many type C grains are nearly homogeneous, but others show roughly concentric zoning. Type C plagioclase shows a moderately well-developed lattice-preferred orientation, but little shape-preferred orientation. This variety of plagioclase occurs only in pseudomorph-bearing Garbenschiefer and in areas where hornblende Garbenschiefer has undergone nearly wholesale conversion to biotite schist.

Textural and chemical evolution of plagioclase

We hypothesize that the three plagioclase types found in the Greiner shear zone formed by different combinations of deformational and metamorphic processes, as illustrated in Fig. 4. The formation of type A plagioclase likely was dominated by prograde metamorphic reactions. In intermediate to mafic bulk compositions, plagioclase with concentric zoning and increasing anorthite content from core to rim is consistent with plagioclase growth during heating and/or decompression into the amphibolite facies (Thompson et al. 1982). Although evidence of climb-accommodated dislocation creep (Hirth and Tullis 1992) exists in type A plagioclase, deformation apparently played a relatively minor role in the initial development of this texture and its associated chemical zoning (Fig. 4a).

In contrast, formation of type B plagioclase was dominated by dissolution-precipitation creep (DPC) following grain-size reduction (Steffen et al. 2001). The DPC regime is favored by small grain size, the presence of a grain-edge fluid phase, and relatively low differential stress (Kerrich et al. 1977; Tullis and Yund 1991; Tullis

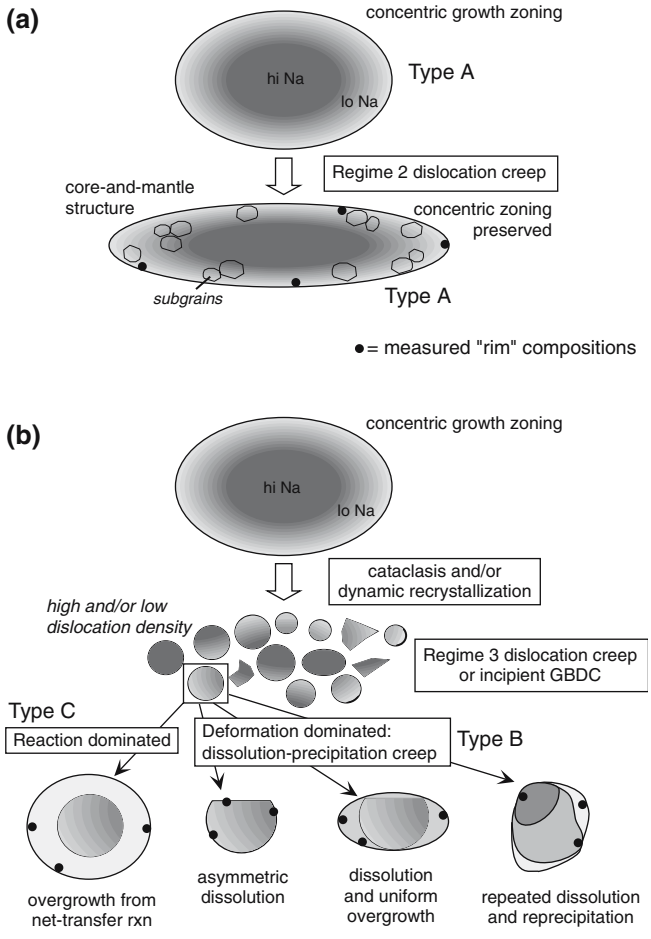

Fig. 4 Model of plagioclase evolution in the Greiner zone. **a** Type A plagioclase develops via growth zoning. Concentric zoning is preserved through modest degrees of climb-accommodated dislocation creep, and rim compositions are homogeneous. **b** Grain-size reduction of type A plagioclase occurs via either cataclasis or dynamic recrystallization and exposes old interior compositions on rims of new grains. Fine grain size can result in strain accommodation by dissolution-precipitation creep. Ongoing DPC results in a range of rim compositions, and youngest composition cannot easily be identified. Net-transfer reactions can accompany DPC and produce both new type C grains and homogeneous overgrowths of type C plagioclase on older cores. *Black dots* represent rim compositions that might be measured for *P–T* calculations; large compositional range will produce a similarly large range in calculated *P* and *T*

et al. 1996), and results in dissolution of material in high-stress areas and reprecipitation in low-stress areas. Nearly dislocation-free grains with complex chemical zoning (Fig. 4b) and no lattice-preferred orientation are produced by this process (Tullis and Yund 1991). Dissolution and reprecipitation typically lead to development of complex chemical zoning patterns involving truncations and localized overgrowths. Experimental studies (Tullis and Yund 1991; Yund and Tullis 1991) of DPC show precipitation of plagioclase of variable and intermediate compositions in an originally bi-compositional system, and data from three natural shear zones show similar compositional effects of DPC (Steffen et al. 2001; Wintsch and Yi 2001; Baxter and DePaolo 2004).

During active DPC, changes in plagioclase composition depend on a combination of metamorphic and deformational factors (Tullis and Yund 1991; Tullis et al. 1996; Wintsch and Yi 2001; Baxter and DePaolo 2004). In rocks with concentrically zoned original plagioclase grains (e.g., type A), grain-size reduction via any mechanism (cataclasis, grain-boundary bulging, or grain-boundary migration recrystallization) exposes interior compositions that were previously chemically isolated by slow intragranular diffusion rates. Dissolution and reprecipitation thus can produce asymmetric chemical zoning patterns composed of original core and rim compositions, as well as the full range of intermediate compositions. Many of these compositions will be out of equilibrium with all other phases in the rock (Fig. 5), and have the potential to provide chemical energy to drive reaction and neocrystallization. DPC may thus increase the kinetics of metamorphic reactions and lead to local production of new plagioclase of intermediate composition (Yund and Tullis 1991). Because this new plagioclase composition decreases the local chemical energy of the system (Fig. 5), its precipitation represents a form of chemically driven GBM. Thus, DPC can change plagioclase composition via a combination of processes driven by both strain energy and chemical energy.

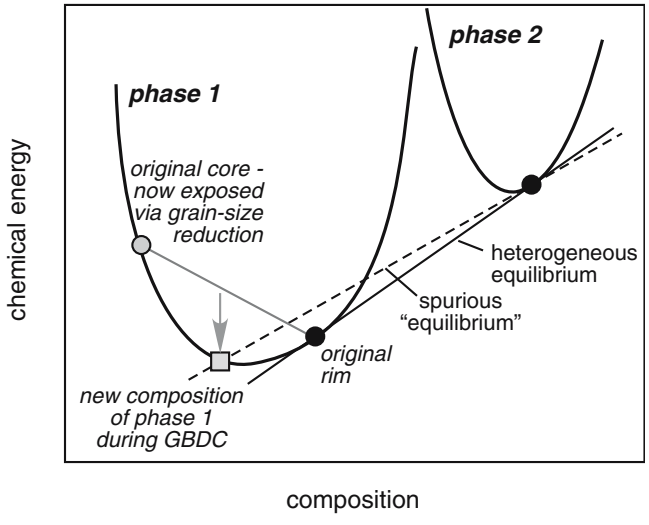

Fig. 5 Schematic chemical energy vs. composition diagram showing the effect of grain-size reduction on local equilibrium in a sample. Rim compositions of phases 1 and 2 are initially in equilibrium with one another. Grain-size reduction exposes disequilibrium core compositions of phase 1. During DPC, dissolution and reprecipitation of phase 1 produces a new, lower energy composition. This composition will be out of equilibrium with phase 2, a mineral that does not undergo DPC. Pairing of the new composition of phase 1 with phase 2 will thus result in spurious calculated *P–T* conditions

The formation of type C plagioclase is dominantly due to metamorphic reaction accompanying chemically driven GBM (Fig. 4b). Type C plagioclase occurs only in areas where hornblende was partially or totally consumed by reactions that converted Al- and K-rich portions of the Garbenschiefer into garnet-biotite schist (hbl + white mica $\rightarrow$ gar + bio + plag $\pm$ epi $\pm$ chl $\pm$ st $\pm$ H_2O; Selverstone and Munoz 1987). The stoichiometry and *P–T* conditions of this reaction in any sample are functions of bulk rock composition, which varies over short distances in the Greiner shear zone. In all cases, however, plagioclase is a reaction product. The weak lattice-preferred orientation of plagioclase suggests nucleation on preexisting grains (Fig. 4b), and the absence of a shape-preferred orientation is consistent with field and petrographic observations that strain was localized into the new biotite-rich horizons during reaction rather than into plagioclase-rich horizons.

The primary method of material transport and strain accommodation during chemically driven GBM and DPC is diffusion along and across grain boundaries. Grain-boundary diffusion is a rate-limiting factor for chemical reaction in most metamorphic rocks (Kretz 1966, 1973; Carlson 2002). Within low-strain domains or between deformation episodes, slow reaction kinetics may prevent the chemical system from fully equilibrating. Stored chemical energy (affinity or ΔG) may build due to *P–T* changes during these periods. At appropriate differential stresses, increased grain boundary diffusion rates will allow strain accommodation by DPC and chemical reaction due to chemically driven GBM. Because of the chemical affinity accumulated in the system, initial reaction rates will be relatively rapid (reaction rate is proportional to affinity for the same kinetic pathway) but will decrease as the system equilibrates. Although strain initially would be required to provide increased diffusion rates and reaction kinetics, GBM may be dominantly driven by chemical affinity stored in the system (Fig. 5). As this stored chemical affinity is consumed, GBM likely would be increasingly driven by DPC.

Retrieval of pressure–temperature data

Methods

Mineral compositions were analyzed with the JEOL 733 electron microprobe in the Department of Earth and Planetary Sciences, University of New Mexico, using operating conditions of 20 keV and 20 nA. A finely focused (~1 μm diameter) beam was used for all analyses,

except for plagioclase in which a defocused (~10 μm diameter) beam was used to minimize Na diffusion under the beam. Natural and synthetic oxides were used as standards and sample compositions were corrected for matrix effects using ZAF procedures. Mineral compositions used in the calculations below are available as electronic supplementary material.

Due to the complexity of plagioclase zoning patterns initially observed using optical microscopy, quantitative electron microprobe traverses were conducted for plagioclase in all samples. The data from these traverses combined with qualitative information derived from BSE images allowed individual plagioclase grains to be categorized into the types described above.

Bulk-rock chemistry (major elements only) was determined using a Rigaku RIX 2100 XRF at the Department of Earth and Planetary Sciences, University of New Mexico. Representative samples were crushed in agate jars in a mixer mill and a mullite mortar and pestle, sieved, and fused into glass disks.

Thermobarometric calculations were performed on 9 sample regions containing varying mineral textures, plagioclase types, and assemblages (Table 1). The purpose of this study is neither to evaluate the accuracy of the thermobarometric calibrations nor to place exact constraints on the *P–T* history of the Greiner zone; rather, we seek to determine how variations in calculated *P–T* conditions reflect the interplay between deformational and metamorphic processes in deep-seated shear zones. In order to explore this variability, we used four different calibrations/approaches: (1) garnet-hornblende thermometry (Graham and Powell 1984), (2) garnet-hornblende-plagioclase-quartz barometry (Kohn and Spear 1989), (3) garnet-biotite-muscovite-plagioclase-quartz barometry (Ghent and Stout 1981), and (4) the AX/Average *P–T* method incorporated in THERMOCALC (Powell and Holland 1994; Powell et al. 1998). The calibrations were applied to all sample regions that contained appropriate assemblages.

In samples that experienced dissolution-precipitation creep of plagioclase (type B), it is generally not possible to determine which composition, if any, equilibrated with other phases in the sample. The selection of a plagioclase composition (Fig. 4b) thus introduces a significant error into the thermobarometric calculations. In order to determine the maximum magnitude of the "plagioclase effect" on retrieved pressure–temperature values, all thermobarometric calculations were performed using four different plagioclase compositions for each sample area: (1) the most albitic composition observed (Ab Max), (2) the most albitic composition observed on a rim (Ab Rim), (3) the most anorthitic composition observed on a rim (An Rim), and (4) the most anorthitic composition observed (An Max). These plagioclase compositions were selected for analysis because they span the total range of compositions present in the samples and also represent the analyses typically used in thermobarometry (rim compositions). With the exception of garnet, other phases present in the samples show little chemical zoning. Garnet compositions used in the calculations were collected from near-rim locations to avoid the effects of retrogression.

Thermobarometric results as a function of plagioclase type and rock texture

Mineral compositions from three groups of samples were used in the thermobarometric calculations in order to assess the influence of textural development and plagioclase type on apparent *P–T* conditions: (1) Garbenschiefer with type A plagioclase (Fig. 6a–c); (2) Garbenschiefer with type B plagioclase (Fig. 6d–f); and (3) Garbenschiefer containing pseudomorphs after hornblende and associated type C plagioclase (Fig. 6g–i). The first group is most similar to the samples used by Selverstone et al. (1984) in that hornblende is stable and plagioclase is concentrically zoned. However, samples used here lack epidote, kyanite, and staurolite, giving them a higher thermodynamic variance than the samples used by Selverstone et al. (1984).

The relative thermobarometric results for the four different plagioclase compositions vary by plagioclase type (Fig. 6). In samples containing concentrically zoned, type A plagioclase, the Ab rim, An Rim, and An Max results cluster together because these compositions tend to be similar; the Ab max composition in these grains typically corresponds solely to mineral cores, and hence yields very different *P–T* results. Calculations using type B plagioclase yield widely scattered results (e.g., Fig. 6g) because dissolution and reprecipitation during DPC resulted in a large range in plagioclase rim

Table 1 Assemblage, texture and plagioclase type

Sample	Plag type	Texture	Hb	Gar	Mu	Pa	Bio	Q	Pl	Chl	Ep	St
BH-00-86-1H2	A–B	GS	X	X			X	X	X	X		
BH-00-86-1K2	A	GS	X	X			X	X	X	X		
FH-00-89-1F	C	PM	X	X			X	X	X	X	X	X
FH-00-810-1A	A–B	GS	X			X	X	X	X	X	X	X
FH-00-810-1H	C	PM	X	X		X	X	X	X			
FH-00-810-1K2	A	GS	X	X			X	X	X	X		
FH-00-810-1L1	C	PM	X	X		X	X	X	X	X	X	
PJ-105-98	A	GS	X	X	X		X	X	X			
99-5-1	B	GS	X	X			X	X	X			

GS Hornblende Garbenschiefer, *PM* pseudomorphs after hornblende Garbenschiefer texture

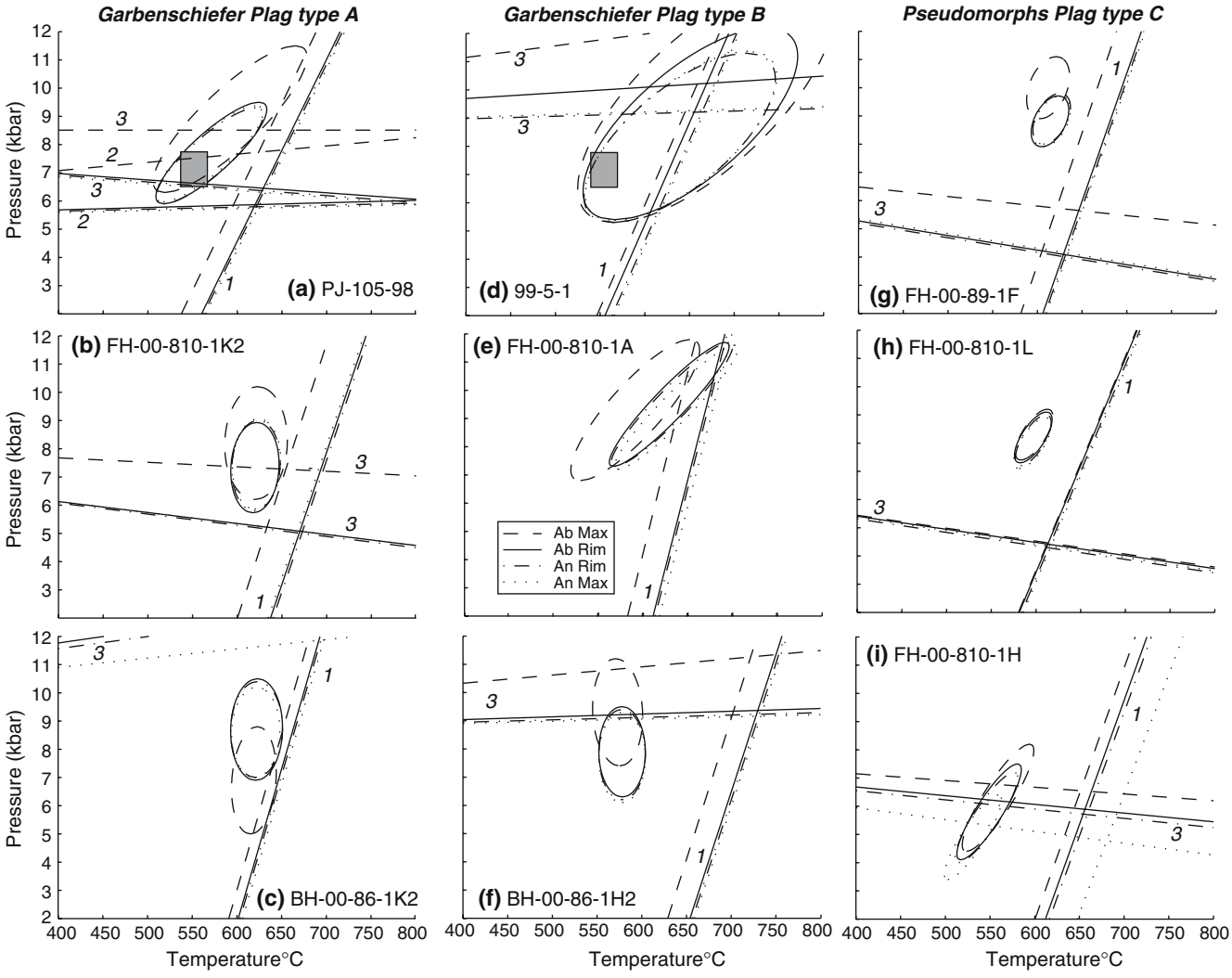

Fig. 6 Thermobarometric results obtained from Garbenschiefer samples containing type A (**a**–**c**) and type B plagioclase (**d**–**f**), and partially pseudomorphed Garbenschiefer containing type C plagioclase (**g**–**i**). **a** and **d** are from westernmost sample localities, and **c** and **f** are from easternmost localities. *Shaded rectangles* in **a** and **c** show final equilibration conditions determined by Selverstone et al. (1984) for western localities. Thermobarometers: *1* hornblende-plagioclase (Holland and Blundy 1994), *2* garnet-biotite-muscovite-plagioclase-quartz (Ghent and Stout 1981), *3* hornblende-garnet-plagioclase-quartz (Kohn and Spear 1989). Ellipses = Average PT/AX method (Powell and Holland 1998). *Ab Max*, *An Max* = the most albitic and most anorthitic plagioclase compositions observed anywhere in a sample. *Ab Rim*, *An Rim* = the most albitic and most anorthitic rim compositions observed in a sample

compositions, even in adjacent grains. Type C plagioclase also produces some scatter in the calculated *P*–*T* conditions (Fig. 6g, i); although most type C grains are relatively homogeneous, some include irregular overgrowths of pseudomorph-related plagioclase on preexisting grains, leading to a larger compositional range.

For calculations using a single thermometer or barometer, the selection of plagioclase compositions within a single sample affects the position of the resulting K_D lines by as much as 2 kbar and 50°C. Plagioclase composition has a somewhat smaller effect on conditions calculated from the Average *P*–*T* multi-equilibrium method (Powell and Holland 1994). The additional constraints provided by equilibria that do not involve plagioclase in the latter method tend to decrease the effects of the extremes in plagioclase composition. Although the variation in calculated *P*–*T* conditions is significant for each sample, the total variation in calculated *P*–*T* conditions for the Greiner shear zone is much larger. For single equilibrium calibrations, calculated conditions span a range of 6 kbar and 175°C. For multi-equilibrium calculations, the variation is approximately 4 kbar and 100°C.

Separation of the thermobarometric data by locality, plagioclase type, or assemblage does not immediately resolve the wide scatter in *P*–*T* results into obvious groups. Limited and differential equilibration of

individual samples at different stages in the deformation and *P–T* history of the Greiner zone certainly affected both mineral chemistry and calculated thermobarometric results, but not in a clear-cut fashion. Below, we use thermodynamic modeling to predict average changes in mineral assemblage, modal abundance, and mineral compositions, and then use this information to identify the features that enhance or inhibit our ability to retrieve meaningful *P–T* data from sheared samples.

Thermodynamic modeling

Predicted equilibrium assemblages for a range of PLSH compositions over the previously determined PTt path (Selverstone et al. 1984) were determined using a pseudosection approach (Steffen 2004). Bulk compositions for two Garbenschiefer samples (one mafic, one intermediate to felsic), a sample with abundant pseudomorphs after hornblende, and a biotite schist were used. Endmember thermodynamic data were taken from Holland and Powell (1998) and the CORK model was used for H_2O (Holland and Powell 1991). Activity-composition models and bulk compositions are listed in the Appendix.

Figure 7a is a pseudosection for the pseudomorph-bearing sample composition, which generally lies between the compositional extremes. The gray lines show the *P–T* path determined by Selverstone et al. (1984) from Gibbs method calculations, inclusion and mineral rim thermobarometry, and fluid-inclusion data. The *P–T* path used in our thermodynamic model was shifted up-temperature by ~35°C relative to the Selverstone et al. (1984) path in order to obtain a better match between observed assemblages and the

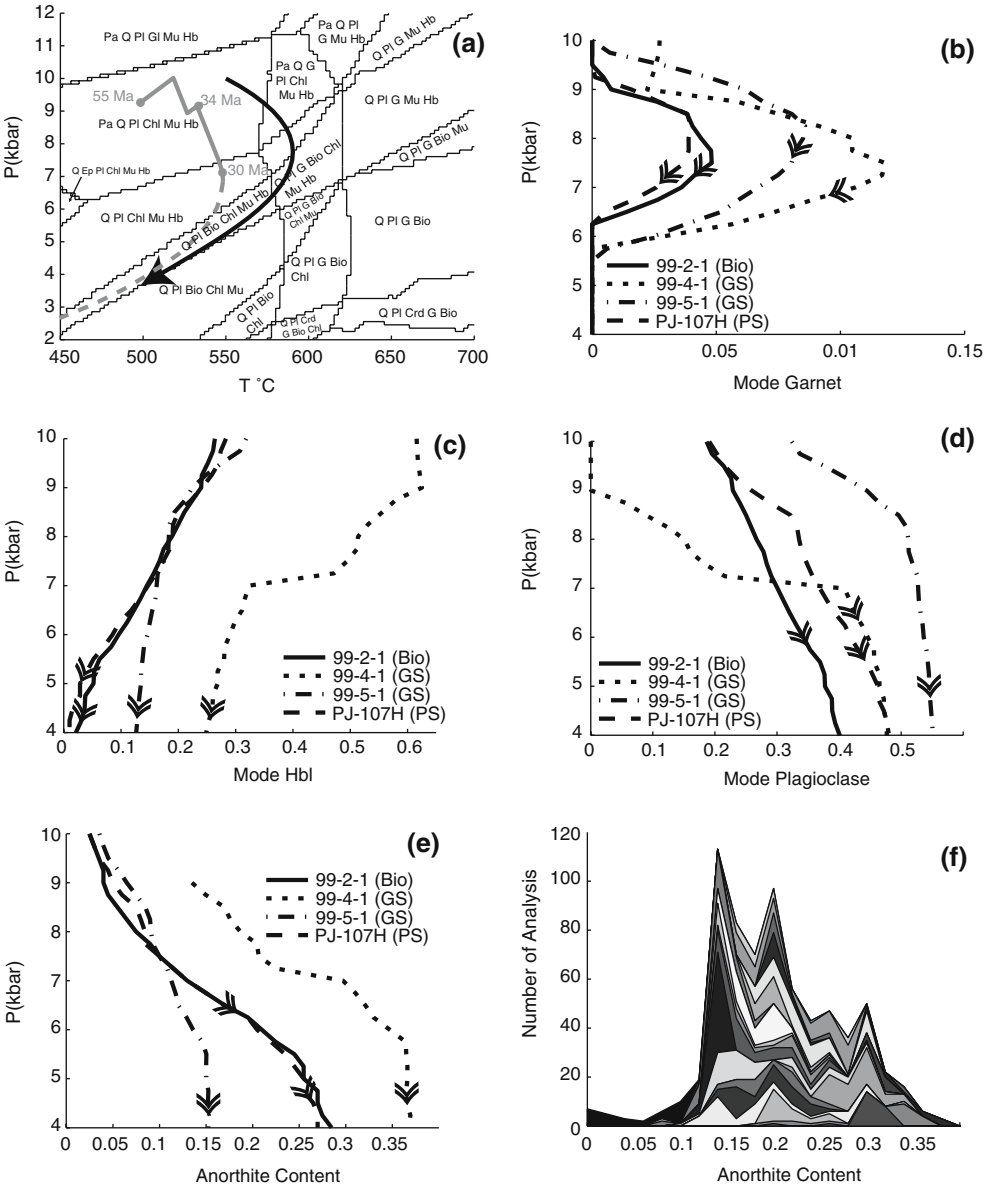

Fig. 7 Thermodynamic modeling results. **a** Pseudosection produced using bulk composition from pseudomorphed Garbenschiefer sample PJ107-H. **b** *Heavy black line* is *P–T* path used for the assemblages calculated in **b–e**. *Heavy gray line* is *P–T* path determined by Selverstone et al. (1984); dates are from Christensen et al. (1994). **b–d** Calculated modes of garnet, hornblende, and plagioclase. **e** Calculated plagioclase composition for all four representative bulk compositions. **f** Histogram of plagioclase compositions collected from 22 sample traverses (697 total analyses)

thermodynamic results (see below). The model predicts garnet growth over a pressure range (10–6 kbar; Fig. 7b) similar to that previously determined by Gibbs method modeling in the PLSH (10-7 kbar, Selverstone et al. 1984). Hornblende mode decreases along this *P–T* path (Fig. 7c) for all samples. The mode of hornblende decreases to less than 3% for the biotite schist and pseudomorph assemblages; continued decompression would decrease the mode of hornblende to zero for these two samples. Because the hornblende-consuming reactions are dehydration reactions, their position in *P–T* space is sensitive to a_{H_2O}; decreasing a_{H_2O} (fixed at unity for these calculations) would shift these reactions to higher pressures and lower temperatures and would decrease the mode of hornblende for all samples.

The equilibrium plagioclase compositions (Fig. 7e) predicted by the model become increasingly anorthitic with decreasing pressure. The predicted increase in plagioclase mode along this *P–T* path would favor the development of growth zoning, with individual grains generally becoming zoned from sodic to more calcic compositions during decompression due to hornblende consumption. These predicted compositions can be compared with all plagioclase data from the natural samples in Fig. 7f (697 spot analyses collected along rim-core-rim plagioclase traverses in 22 different sample regions; note that although there are modes in the histogram, there is also continuous variation in plagioclase composition and no evidence in the data for a solvus). For type A and type C plagioclase, core compositions are always more sodic than the rims; truncations in type B plagioclase grains make it difficult to interpret the relative ages of different compositions. Nonetheless, there is good agreement between the actual plagioclase compositions and the trends predicted by Fig. 7d and e for each of the different modeled bulk compositions. The wide range in plagioclase compositions within each sample can thus be largely ascribed to differential equilibration and development of growth zoning during decompression.

In summary, the thermodynamic modeling indicates that hornblende abundance should decrease, plagioclase mode should increase, and plagioclase should become increasingly calcic along a *P–T* path similar to that determined by Selverstone et al. (1984). Plagioclase produced by reaction should thus become more anorthitic with time. However, DPC will tend to expose cores of previously zoned grains, and hence will lower the anorthite content to a value that is less than the predicted equilibrium composition. These results are consistent with plagioclase zoning patterns observed in the Greiner shear zone. Because all relevant chemical reactions produce increasingly anorthitic plagioclase, the appropriate composition to use in thermobarometric calculations in these rocks is the most anorthitic one, even if that composition is not a rim composition. For samples that were not significantly affected by DPC, plagioclase is concentrically zoned and the An Max composition is similar to the rim compositions that would typically be used for thermobarometry.

Multi-equilibrium results derived from An Max values

The An Max plagioclase composition in each sample area was used to calculate *P–T* conditions for stable Garbenschiefer and partially pseudomorphed samples via the Average *P–T* routine in THERMOCALC (Powell and Holland 1994; Fig. 8). The calculated conditions span the range calculated by Selverstone et al. (1984), though shifted to higher temperatures (likely reflecting the use of different thermodynamic datasets). Although there is considerable scatter in the data overall, the results show reasonable overlap for each rock type. In particular, they show considerably less variability than the results shown in Fig. 6, which utilized a range of different plagioclase compositions. The largest error ellipse, however, remains associated with type B plagioclase.

In general, if the fit/fit cutoff ratio for the multi-equilibrium calculations exceeds 1.0, the calculated *P–T* conditions are not internally consistent for the selected activity and enthalpy uncertainty values (Powell and Holland 1994). Fit/fit cutoff values between 1.0 and 1.5 for the Greiner samples indicate that the mineral compositions used in this study generally yield Average *P–T* values that are not internally consistent. Increasing the uncertainties in the activity (calculated in AX) and enthalpy input would make the calculations consistent, but would also increase the size of the uncertainty ellipse.

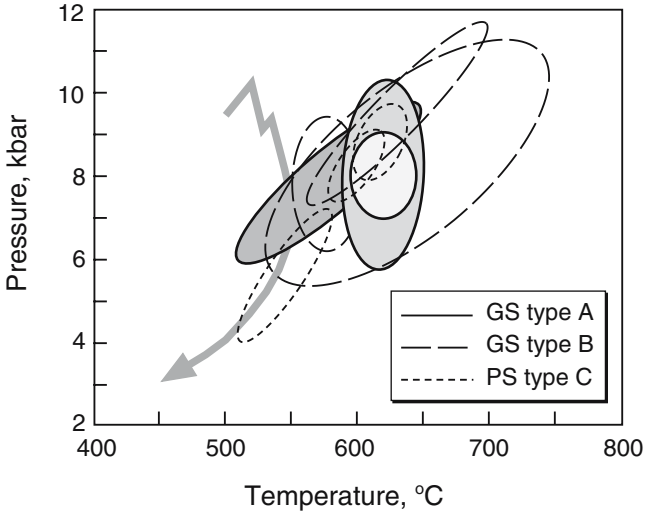

Fig. 8 Results of multi-equilibrium calculations (Average PT; Holland and Powell 1994) using just An Max compositions. *GS* Garbenschiefer with type A or B plagioclase; *PS* samples with pseudomorphs after hornblende that contain type C plagioclase. Ellipses for type A plagioclase are shaded for ease of reading. Note large ellipses associated with type B plagioclase, and small ellipses but scattered *P–T* results for samples containing pseudomorphs; the former represents disequilibrium, whereas the latter represents equilibration at different sets of *P–T* conditions. *Arrowed P–T* path is from Selverstone et al. (1984)

There are two potential sources for the poor consistency recorded by these samples: (1) The endmember thermodynamic data of Powell and Holland (1998) and the activity-composition models used by AX may be significantly in error. Although possible, we consider this explanation unlikely: other studies have applied the same endmember data and activity-composition models to samples with similar assemblages and obtained consistent results (Puga et al. 2000; Dale and Holland 2003). (2) Disequilibrium between minerals in the samples also can lead to inconsistency. The generally accepted approach to evaluating the role of disequilibrium in multi-equilibrium thermobarometry is to remove activities of certain endmembers from consideration using statistics provided by the program (see Powell and Holland 1994, for details). However, in our samples, removing various endmembers from consideration did not significantly improve the consistency of the results. In particular, no specific endmember could be identified whose activities contributed the largest portion of the inconsistency. These results indicate that the samples used in this study generally fail the assumption of local equilibrium, rather than recording the metastable persistence of a single phase. Relative timing of equilibration, likely related to the relative timing of strain localization events, appears to have exerted the dominant control on chemical equilibration. Although all samples in the Greiner shear zone experienced the same overall *P–T* history, the calculated *P–T* conditions were frozen in at very different times in different sample areas, depending on local variations in bulk composition, reaction rates, fluid mobility, and mechanisms of strain accommodation (e.g., Fig. 4). In addition to choosing appropriate mineral compositions for thermobarometry within individual samples, it is thus also necessary to choose a sample suite recording a wide range of metamorphic and deformational features when attempting to retrieve *P–T* information from shear zones.

Linked metamorphism and deformation in the Greiner shear zone

In horizons where coarse hornblende developed relatively early, the interlocking hornblende grains caused

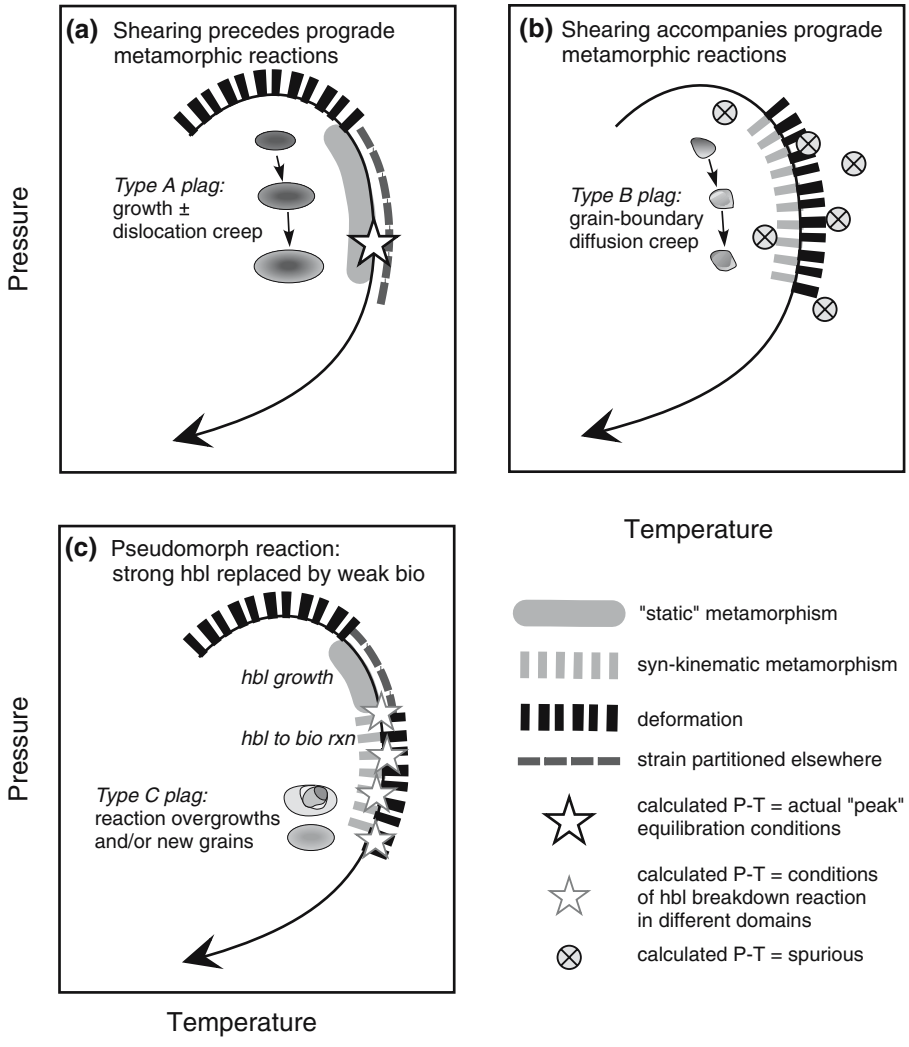

Fig. 9 Schematic diagrams showing consequences of differences in relative timing of prograde metamorphism, deformation, changes in plagioclase deformation mechanism, and hornblende breakdown for calculated *P–T* conditions. **a** Samples that underwent early shearing followed by growth of type A plagioclase yield consistent information on thermal peak of metamorphism. **b** Samples that experienced strain accommodation via grain-boundary diffusion creep near thermal maximum yield scattered *P–T* results owing to chaotic zoning produced in plagioclase. **c** Breakdown of hornblende to produce biotite and type C plagioclase occurred at different conditions in different samples, and hence a variety of *P–T* conditions will be calculated. Once biotite was produced, strain was localized back into these samples

later deformation to be partitioned into other domains within the shear zone (Steffen et al. 2001). As the *P–T* path neared the thermal maximum, plagioclase continued to grow in these horizons but there was relatively little synchronous strain accumulation. Hence, metamorphic processes dominated over deformational processes, and plagioclase developed concentric growth zoning (type A; Fig. 9a). Thermobarometric calculations in these strong domains yield reliable *P–T* conditions with relatively small scatter.

In horizons where grain-size reduction occurred closer to the thermal maximum, the Garbenschiefer texture developed later than in the example above. Grain-size reduction resulted in strain accommodation by DPC, producing type B plagioclase (Steffen et al. 2001). In these samples, there was insufficient time for the plagioclase to be modified by metamorphic reactions near T_{max}, and chaotic DPC zoning was preserved (Fig. 9b). Thermobarometric calculations thus return meaningless *P–T* values.

Rocks exhibiting pseudomorphs after hornblende contain type B and type C plagioclase. In these samples, the Garbenschiefer texture formed early in concert with DPC but was later destabilized by metamorphic reactions (Fig. 9c). The destruction of the Garbenschiefer framework weakened the domains and allowed strain to affect the plagioclase, leading to the formation of type B plagioclase in addition to the type C plagioclase created by the reactions that consume hornblende. In biotite schist domains, the rocks never strengthened and deformation and metamorphism interacted throughout the *P–T* path.

In diffusion-limited systems, reaction kinetics are dominated by thermally activated diffusion rates and this relationship explains why thermobarometric calculations using rim compositions yield conditions of the thermal maximum. In our model, static metamorphism at the thermal maximum is relevant only for stable Garbenschiefer with type A plagioclase (Fig. 9a). The samples used by Selverstone et al. (1984) were of this texture and produced thermobarometric results for rim compositions that showed little variation within or between samples. Thermobarometric results obtained in this study for this texture also show relatively low scatter of approximately ± 50°C and ± 1.5 kbar [with the exception of the results for sample BH-00-86-1K2 in Fig. 6c; sodic plagioclase in this sample is out of the range suggested for the Kohn and Spear (1989) calibration and is likely a remnant high-P composition].

For other textures and plagioclase types, deformational and metamorphic processes were both active near the thermal maximum, and deformation likely had a strong effect on grain-boundary diffusion rates and reaction kinetics. The pressures calculated from rim compositions in these samples span the decompression path calculated by Selverstone et al. (1984) from zoned minerals. Episodes of strain localization in these samples would have caused transient increases in diffusion rates and rates of mineral equilibration. Because equilibration rates were likely slower during slow strain-rate periods, the mineral compositions produced during deformation were unlikely to be significantly reset by diffusion and reaction at the thermal maximum. Thermobarometric calculations on many of these rocks thus yield *P–T* conditions related to discrete episodes of strain localization, and not necessarily to the maximum temperature attained by the rocks.

Implications and recommendations for *P–T* calculations in shear zones

Transient changes in reaction rates due to the combined effects of metamorphism and deformation may fundamentally affect the accuracy of thermobarometric results. In cases of "static" metamorphism, where diffusion rates depend primarily on temperature, reaction rates should co-vary with temperature. Because temperature changes will be limited by the thermal conductivity of the surrounding rocks, changes in reaction rates are predicted to occur gradually. During synmetamorphic deformation, however, strain localization and/or changes in deformation mechanism related to high strain-rate events can strongly influence reaction rates and kinetic pathways. The combined spatial and temporal variations in reaction rates may result in situations in which chemical equilibrium is only attained for certain components or phases, or only in local domains. Preservation of the resulting compositional heterogeneities will contribute to poor consistency and/or meaningless calculated *P–T* conditions (Fig. 9b).

The activation of different deformation mechanisms can lead to the formation of mineral zoning patterns that are difficult to interpret and lend large geologic uncertainty to thermobarometric calculations. In general, fine-grained samples that experience dissolution-precipitation creep are likely to be the most problematic owing to the discontinuous zoning that can develop. In these samples, the most evolved mineral composition (An Max in this study) should be used in *P–T* calculations, even if that composition is not a rim composition. In some cases, even this composition may not have been in local equilibrium with other phases in the rock (Fig. 6).

Determination of the most-evolved mineral composition requires thermodynamic modeling of the bulk rock in order to identify the key continuous equilibria that operated and their predicted effects on mineral compositions. Construction of pseudosections with THERMOCALC or other programs can give a general sense of the pressure–temperature conditions that prevailed during synmetamorphic deformation. However, pseudosections are generally calculated for relatively simple chemical systems and also do not take into account changes in effective bulk composition arising from development of chemical zoning. As a result, the use of pseudosections does not completely replace standard thermobarometric methods. Based on the results of this

study, we recommend the use of pseudosection calculations primarily to predict the most evolved mineral compositions that should develop during synmetamorphic deformation in a rock of a particular bulk composition. Once that general composition has been identified (e.g., the most An-rich plagioclase or the most Fe-rich garnet), microprobe data should be used to determine specific mineral compositions for thermobarometry.

In shear zones that experience protracted deformation histories, the relative timing of textural development and chemical equilibration can produce large variations in calculated P and T within and between samples. In the Greiner shear zone, samples that were little affected by deformation at conditions near the maximum temperature yield P–T results that are more internally consistent than results from samples that experienced shear localization at or near the thermal maximum. Some of the scatter likely represents real spatial variation in the P–T conditions at which equilibration occurred within the shear zone. However, the large variation in calculated P–T conditions within and between samples containing plagioclase that underwent dissolution and reprecipitation suggests that many of the thermobarometric results are spurious and reflect short-lived, deformation-induced chemical heterogeneities.

Retrieval of meaningful P–T data from sheared samples thus requires detailed assessment of the interactions between strain accommodation mechanisms and chemical equilibration at both the field and microscopic scales. In general, analysis of mineral deformation mechanisms should be coupled with thermodynamic modeling to place constraints on the entire P–T interval over which deformation occurred. Individual thermobarometers are unlikely to provide meaningful PTt histories if dissolution-precipitation creep of zoned minerals was activated during shearing.

Acknowledgements This research was funded by NSF grant EAR-0000965 to J. Selverstone and A. Brearley, a Kelley-Silver Graduate Fellowship and a Vincent Kelley Scholarship (Steffen) from the Department of Earth & Planetary Sciences at the University of New Mexico, a Mineralogy/Petrology Research Grant from the Mineralogical Society of America (Steffen), and a Student Research Grant in Mathematical Geology from the International Association of Mathematical Geology (Steffen). Micah Jessup, Aaron Cavosie, Jaime Barnes, and Amanda Tyson provided able field assistance. We thank journal reviewers Ethan Baxter and, especially, Jan Tullis for their constructive comments on the manuscript.

Appendix: Mineral activity models and bulk compositions

Activity-composition models used in thermodynamic model (Fig. 7) Endmember thermodynamic data from Holland and Powell (1998), water model using CORK (Holland et al. 1998)

Bulk compositions used in thermodynamic modeling

Phase	Model
Paragonite	Unit activity
Lawsonite	Unit activity
Quartz	Unit activity
Water	Unit activity
Kyanite	Unit activity
Sillimanite	Unit activity
Andalusite	Unit activity
Prehnite	Unit activity
Pumpellyite	Unit activity
Epidote	Unit activity, clinozoisite
Plagioclase	DQF model (Holland and Powell 1992)
Cordierite	Ideal crd, fcrd, site multiplicity = 2
Chloritoid	Ideal mctd, fctd, site multiplicity = 1
Carpholite	Ideal mcar, fcar, site multiplicity = 1
Staurolite	Ideal mst, fst, site multiplicity = 4
Spinel	Ideal sp, herc, site multiplicity = 1
Omphacite	DQF omph, feomph, di, hed (di 20,000 J/m, hed 20,000 J/m)
Garnet	Non-ideal gr, alm, py (Dale et al. 2000)
Chlorite	Disordered clin, daph, ames parameters from (Holland et al. 1998)
Muscovite	Mu, cel, fecel, pa, Mu–cel–fel parameters from (Coggon and Holland 2002), exchange to paragonite by DQF (pa 20,000 J/m)
Biotite	Non-ideal phl, ann, east disordered (Powell and Holland 1999)
Hornblende	tr, fact, ts, fets, gl, fegl, parg, feparg, DQF model (tr 46,000 J/m, fact 35,000 J/m, gl 32,000 J/m, fegl 16,000 J/m, parg 20,000 J/m, feparg 32,000 J/m). Values modified to create hornblende compositions similar to those observed in natural samples.
Glaucophane	Non-ideal tr, ts, fact, gl (Dale et al. 2000)

Sample	SiO_2	Al_2O_3	FeO	MgO	CaO	Na_2O	K_2O
99-2-1	59.58	16.77	8.87	3.81	2.55	3.22	2.86
99-4-1	49.58	19.35	12.64	5.61	6.51	3.69	0.60
99-5-1	65.60	14.72	7.36	2.45	3.27	5.48	0.11
PJ107-H	59.87	17.38	7.76	3.66	2.72	3.90	2.09

99-2-1 = biotite schist, 99-4-1 = Garbenschiefer, 99-5-1 = Garbenschiefer, PJ-107H = pseudomorph-bearing sample

References

Arnold J, Powell R, Sandiford M (2000) Amphibolites with staurolite and other aluminous minerals: calculated mineral equilibria in NCFMASH. J Metamorph Geol 18:23–40

Baxter EF, DePaolo DJ (2004) Can metamorphic reactions proceed faster than bulk strain. Contrib Mineral Petrol 146:657–670

Brodie KH (1981) Variation in amphibole and plagioclase composition with deformation. Tectonophysics 78:385–402

Brodie KH, Rutter EH (1985) On the relationship between deformation and metamorphism, with special reference to the behavior of basic rocks. In: Thompson AB, Rubie DC (eds) Metamorphic reactions. Springer, Berlin Heidelberg New York, pp 138–179

Carlson WD (2002) Scales of disequilibrium and rates of equilibration during metamorphism. Am Mineral 87:185–204

Chernoff CB, Carlson WD (1997) Disequilibrium for Ca during growth of pelitic garnet. J Metamorph Geol 15:421–438 University of Texas at Austin, Department of Geological Sciences, Austin, TX, United States

Coggon R, Holland T (2002) Mixing properties of phengitic micas and revised garnet-phengite thermobarometers. J Metamorph Geol 20:683–696

Dale J, Holland T (2003) Geothermobarometry, *P–T* paths and metamorphic field gradients of high-pressure rocks from the Adula Nappe, Central Alps. J Metamorph Geol 21:813–829

Dale J, Holland T, Powell R (2000) Hornblende-garnet-plagioclase thermobarometry: a natural assemblage calibration of the thermodynamics of hornblende. Contrib Mineral Petrol 140:353–362

Farver J, Yund R (1999) Oxygen bulk diffusion measurements and TEM characterization of a natural ultramylonite: implications for fluid transport in mica-bearing rocks. J Metamorph Geol 17:669–683

Frost R, Tracy RJ (1991) *P–T* paths from zoned garnets; some minimum criteria. Am J Sci 291:917–939

Ghent ED, Stout MZ (1981) Geobarometry and geothermometry of plagioclase-biotite-garnet-muscovite assemblages. Contrib Mineral Petrol 76:92–97

Graham C, Powell R (1984) A garnet-hornblende geothermometer: calibration, testing, and application to the Pelona Schist. J Metamorph Geol 2:13–21

Hirth G, Tullis J (1992) Dislocation creep regimes in quartz. J Struct Geol 14:145–159

Holland T, Baker J, Powell R (1998) Mixing properties and activity-composition relationships of chlorites in the system $MgO–FeO–Al_2O_3–SiO_2–H_2O$. Eur J Mineral 10:395–406

Holland T, Powell R (1991) A Compensated-Redlich-Kwong (CORK) equation for volumes and fugacities of CO_2 and H_2O in the range 1 bar to 50 kbar and 100–1600°C. Contrib Mineral Petrol 109:265–273

Holland T, Powell R (1992) Plagioclase feldspars: activity-composition relations based upon Darken's quadratic formalism and Landau theory. Am Mineral 77:53–61

Holland T, Powell R (1998) An internally consistent data set for phases of petrologic interest. J Metamorph Geol 16:309–343

Kerrich R, Beckinsale RD, Durham JJ (1977) The transition between deformation regimes dominated by intercrystalline diffusion and intracrystalline creep evaluated by oxygen isotope thermometry. Tectonophysics 38:241–257

Kohn MJ, Spear FS (1989) Empirical calibration of geobarometers for the assemblage garnet + hornblende + plagioclase + quartz. Am Mineral 74:77–84

Kohn MJ, Spear FS (1991) Error propagation for barometers 2: application to rocks. Am Mineral 76:138–147

Koons PO, Rubie DC, Frueh-Green G (1987) The effects of disequilibrium and deformation on the mineralogical evolution of quartz diorite during metamorphism in the eclogite facies. J Petrol 28:679–700 ETH-Zentrum, Dep. Erdwissenschaften, Zurich, Switzerland

Kretz R (1966) Grain-size distribution for certain metamorphic minerals in relation to nucleation and growth. J Geol 74:147–173

Kretz R (1973) Kinetics of the crystallization of garnet at two localities near Yellowknife. Can Mineral 12:1–20

Lammerer B (1988) Thrust-regime and transpression-regime tectonics in the Tauern Window (Eastern Alps). Geol Rund 77:143–156

Lammerer B, Weger M (1998) Footwall uplift in an orogenic wedge: the Tauern Window in the Eastern Alps of Europe. Tectonophysics 285:213–230

Morteani G (1974) Petrology of the Tauern Window, Austrian Alps. Fortschr Mineral 52:195–220

Powell R, Holland T (1994) Optimal geothermometry and geobarometry. Am Mineral 79:120–133

Powell R, Holland T (1999) Relating formulations of the thermodynamics of mineral solid solutions: activity modeling of pyroxenes, amphiboles, and micas. Am Mineral 84:1–14

Powell R, Holland T, Worley B (1998) Calculating phase diagrams involving solid solutions via non-linear equations, with examples using THERMOCALC. J Metamorph Geol 16:577–588

Puga E, Nieto JM, De Federico AD (2000) Contrasting *P–T* paths in eclogites of the Betic Ophiolitic Association, Mulhacen Complex, southeastern Spain. Can Mineral 38:1137–1161

Ratschbacher L, Merle O, Davy P, Cobbold P (1991) Lateral extrusion in the eastern Alps; 1. Boundary-conditions and experiments scaled for gravity. Tectonics 10:245–256

Selverstone J (1985) Petrologic constraints on imbrication, metamorphism, and uplift in the SW Tauern Window, Eastern Alps. Tectonics 4:687–704

Selverstone J (1988) Evidence for east-west crustal extension in the Eastern Alps: Implications for the unroofing history of the Tauern Window. Tectonics 7:87–105

Selverstone J (1993) Microscale to macroscale interactions between deformational and metamorphic processes, Tauern-Window, Eastern Alps. Schweiz Mineral Petrograph Mitt 73:229–239

Selverstone J, Munoz JL (1987) Fluid heterogeneities and hornblende stability in interlayered graphitic and nongraphitic schists (Tauern Window, Eastern Alps). Contrib Mineral Petrol 96:426–440

Selverstone J, Spear FS, Franz G, Morteani G (1984) High-pressure metamorphism in the SW Tauern Window, Austria: *P–T* paths from hornblende-kyanite-staurolite schists. J Petrol 25:501–531

Spear FS, Selverstone J (1983) Quantitative *P–T* paths from zoned minerals: theory and tectonic applications. Contrib Mineral Petrol 83:348–357

Steffen K, Selverstone J, Brearley A (2001) Episodic weakening and strengthening during synmetamorphic deformation of a deep crustal shear zone in the Alps. In: Holdsworth RE, Strachan RA, Magloughlin JF, Knipe RJ (eds) The nature and tectonic significance of fault zone weakening. The Geological Society of London, London, pp 141–156

Steffen KJ (2004) Automation of phase classification, calculation of metastable chemical energy, and the interaction of deformational and metamorphic processes. In: Earth and Planetary Sciences. University of New Mexico, Albuquerque, pp 508

Stünitz H (1998) Syndeformational recrystallization: dynamic or compositionally induced. Contrib Mineral Petrol 131:219–236

Stünitz H, Tullis J (2001) Weakening and strain localization produced by syn-deformational reaction of plagioclase. Int J Earth Sci 90:136–148

Stüwe K (1997) Effective bulk composition changes due to cooling: a model predicting complexities in retrograde reaction textures. Contrib Mineral Petrol 129:43–52

Thompson JB, Laird J, Thompson AB (1982) Reactions in amphibolite, greenschist and blueschist. J Petrol 23:1–27

Tracy RJ (1976) Garnet compositions and zoning in the determination of temperature and pressure of metamorphism, Central Massachusetts. Am Mineral 61:762–775

Tracy RJ (1982) Compositional zoning and inclusions in metamorphic minerals. In: Ferry JM (ed) Characterization of metamorphism through mineral equilibria. Mineralogical Society of America, Washington, pp 355–397

Tullis J, Yund R, Farver J (1996) Deformation-enhanced fluid distribution in feldspar aggregates and implications for ductile shear zones. Geology 24:63–66

Tullis J, Yund RA (1991) Diffusion creep in feldspar aggregates: experimental evidence. J Struct Geol 13:987–1000

Wintsch RP, Knipe RJ (1983) Growth of a zoned plagioclase porphyroblast in a mylonite. Geology 11:360–363

Wintsch RP, Yi K (2001) Dissolution and replacement creep: a significant deformation mechanism in mid-crustal rocks. J Struct Geol 24:1179–1193

Yardley B, Rochelle CA, Barnicoat AC, Lloyd GE (1991) Oscillatory zoning in metamorphic minerals—an indicator of infiltration metasomatism. Mineral Mag 55:357–365

Yund RA, Tullis J (1991) Compositional changes of minerals associated with dynamic recrystallization. Contrib Mineral Petrol 108:346–355